Setting the scale for the CLS $2 + 1$ flavor ensembles

Mattia Bruno[a,b], Tomasz Korzec[c], Stefan Schaefer[a]

[a] John von Neumann Institute for Computing (NIC), DESY
Platanenallee 6, D-15738 Zeuthen, Germany
[b] Physics Department, Brookhaven National Laboratory, Upton, NY 11973, USA
[c] Department of Physics, Bergische Universität Wuppertal
Gaussstr. 20, D-42119, Wuppertal, Germany

Abstract

We present measurements of a combination of the decay constants of the light pseudoscalar mesons and the gradient flow scale t_0, which allow to set the scale of the lattices generated by CLS with $2 + 1$ flavors of non-perturbatively improved Wilson fermions. Mistunings of the quark masses are corrected for by measuring the derivatives of observables with respect to the bare quark masses.

1   Introduction

A lattice scale is a dimensionful quantity which can be used to form dimensionless ratios of observables with a well-defined continuum limit. In principle, its choice is arbitrary, however, the precision to which we can extract the scale on the lattice and the accuracy, to which its experimental value is known, will affect the precision of the final results.

Here, we will determine two such scales for the setup chosen in the CLS simulations with $N_{\rm f} = 2 + 1$ flavors of $O(a)$ improved Wilson fermions and the tree-level Lüscher–Weisz gauge action, which has been described in detail in Ref. [1]. The two scales are a combination of the pseudoscalar decay constants f_π and $f_{\rm K}$ as well as t_0, the gluonic dimension two quantity introduced by Lüscher in Ref. [2] using the Wilson flow.

Other observables commonly used in scale setting are the mass of the Ω^- baryon [3], the Υ-Υ' mass splitting [4] or the scale r_0 [5] defined from the force between two static quarks. For the latter, like for t_0, the physical value is not known from experiment, but has to be computed on the lattice. Still such quantities can be very useful as intermediate scales due to their high statistical accuracy and the fact that their definition does not include valence quarks. This makes them also useful in studies which connect results with different flavor content in the sea. The study presented here is in some aspects similar to the one by QCDSF [6], where combinations of hadron masses are used to set the scale in the determination of t_0.

The results of lattice QCD simulations are dimensionless ratios of observables. Since we restrict ourselves to three flavors, with the two light ones degenerate, these ratios will differ from those found in Nature. Therefore the choice of input observable will affect the global normalization of the results. However, the scale also enters in the definition of the physical quark mass point and therefore also directly affects the ratios of observables. Because of the latter, $N_{\rm f} = 2 + 1$ flavor results become unique only after specifying the lattice scale and the observables used to set the quark masses. Deviations from uniqueness, however, are very small effects as long as one remains in the low energy sector of the theory where decoupling holds [7].

The paper is organized as follows: In Section 2 we first give a brief overview of the ensembles as well as the observables we consider. Section 3 discusses the issues which occur in the extraction of the masses and matrix elements in the presence of open boundary conditions in time, as used in the CLS simulations. In Section 4 the method to correct for mistunings by using mass derivatives of the observables is detailed, before presenting the results in Section 5 and concluding.

2   Setup

We want to set the scale for the ensembles generated by the CLS 2+1 effort which use the tree-level $O(a^2)$ improved Lüscher-Weisz gauge action and improved Wilson fermions with a non-perturbative $c_{\rm sw}$ [8]. Three values of the coupling have been

id	β	N_s	N_t	κ_u	κ_s	$m_\pi[\mathrm{MeV}]$	$m_K[\mathrm{MeV}]$	$m_\pi L$
H101	3.40	32	96	0.13675962	0.13675962	420	420	5.8
H102	3.40	32	96	0.136865	0.136549339	350	440	4.9
H105	3.40	32	96	0.136970	0.13634079	280	460	3.9
C101	3.40	48	96	0.137030	0.136222041	220	470	4.7
H400	3.46	32	96	0.13688848	0.13688848	420	420	5.2
H401	3.46	32	96	0.136725	0.136725	550	550	7.3
H402	3.46	32	96	0.136855	0.136855	450	450	5.7
H200	3.55	32	96	0.137000	0.137000	420	420	4.3
N202	3.55	48	128	0.137000	0.137000	420	420	6.5
N203	3.55	48	128	0.137080	0.136840284	340	440	5.4
N200	3.55	48	128	0.137140	0.13672086	280	460	4.4
D200	3.55	64	128	0.137200	0.136601748	200	480	4.2
N300	3.70	48	128	0.137000	0.137000	420	420	5.1
J303	3.70	64	192	0.137123	0.1367546608	260	470	4.1

Table 1: List of the ensembles. In the id, the letter gives the geometry, the first digit the coupling and the final two label the quark mass combination.

employed $\beta = 3.4$, 3.55 and 3.7, which correspond roughly to a lattice spacing of $a = 0.085\,\mathrm{fm}$, $0.065\,\mathrm{fm}$ and $0.05\,\mathrm{fm}$, respectively. Data limited to degenerate quark masses is also available at $\beta = 3.46$. An overview can be found in Tab. 1, with ensemble N203 first described in Ref. [9].

Apart from $\beta = 3.46$, these ensembles lie along lines of constant sum of the bare quark masses $m_\mathrm{q} = (1/\kappa_\mathrm{q} - 8)/2$ with degenerate light quarks $m_\mathrm{ud} \equiv m_\mathrm{u} = m_\mathrm{d}$ and an average quark mass m_sym. κ_q is the standard hopping parameter of the Wilson quark action [10]. Using the quark mass matrix $M_\mathrm{q} = \mathrm{diag}(m_\mathrm{u}, m_\mathrm{d}, m_\mathrm{s})$, we therefore have

$$3m_\mathrm{sym} = \mathrm{tr}\, M_\mathrm{q} = 2m_\mathrm{ud} + m_\mathrm{s} = \mathrm{const}\,. \qquad (2.1)$$

This line has been chosen, because it implies a constant $\mathrm{O}(a)$ improved coupling [11]

$$\tilde{g}_0^2 = g_0^2 \left(1 + \frac{1}{3} b_\mathrm{g}\, a \,\mathrm{tr}\, M_\mathrm{q}\right), \qquad (2.2)$$

irrespective of the knowledge of the improvement coefficient b_g.

To further specify the chiral trajectories, we have to define a point in the $(m_\mathrm{ud}, m_\mathrm{s})$ plane through which it is supposed to pass. To this end, we have used the dimensionless variables

$$\phi_2 = 8\, t_0\, m_\pi^2 \qquad \text{and} \qquad \phi_4 = 8\, t_0\, (m_\mathrm{K}^2 + \frac{1}{2} m_\pi^2) \qquad (2.3)$$

with the requirement that the chiral trajectory intersects the symmetric line $m_\mathrm{ud} = m_\mathrm{s}$ at $\phi_4 = 1.15$. Here, m_π and m_K are the masses of the pseudoscalars corresponding

to the pion and the kaon. The value of $\phi_4 = 1.15$ comes from a preliminary analysis of the quark mass dependence of ϕ_4; only the final analysis can tell in how far this chiral trajectory goes through the point of physical ϕ_4 and ϕ_2.

Three points in this strategy need special attention: First of all, eq. (2.1) does not imply a constant sum of renormalized quark masses, which is already violated to O(a)

$$\mathrm{tr}\ M^{\mathrm{R}} = Z_{\mathrm{m}} r_{\mathrm{m}} [(1 + a\bar{d}_{\mathrm{m}} \mathrm{tr}\, M_{\mathrm{q}}) \mathrm{tr}\, M_{\mathrm{q}} + a d_{\mathrm{m}} \mathrm{tr}\, M_{\mathrm{q}}^2] \,, \tag{2.4}$$

as worked out in Ref. [12], whose notation we are using. Secondly, the tuning in ϕ_4 is correct only up to a certain degree and it is at the current stage by no means clear that the thus defined trajectories also go through the physical quark mass points. The potential mistuning needs to be taken into account in the analysis.

Furthermore, the definition of the point of physical quark masses depends at physical lattice spacing on the scale. The tuning has been done using t_0 for which the precise experimental value is not known. It might therefore be preferable to use the decay constants also at finite lattice spacing, but this will necessarily lead to chiral trajectories which are no longer matched to the same level of accuracy.

2.1   Observables

The physical quantity used here to convert the lattice measurements to physical units is the combination of the pseudoscalar decay constants of pion f_π and kaon f_{K}, which along with its next to leading order expansion in SU(3) chiral perturbation theory [13] is given by

$$
\begin{aligned}
f_{\pi\mathrm{K}} &\equiv \frac{2}{3}\left(f_{\mathrm{K}} + \frac{1}{2}f_\pi\right) \\
&\approx f\left[1 - \frac{7}{6}L_\pi - \frac{4}{3}L_{\mathrm{K}} - \frac{1}{2}L_\eta + \frac{16B\,\mathrm{tr}\,M}{3f^2}(L_5 + 3L_4)\right] \,.
\end{aligned}
\tag{2.5}
$$

The a priori unknown low energy constants L_4 and L_5 appear only in the $\mathrm{tr}\,M$ term and logarithms are given by $L_x = m_x^2/(4\pi f)^2 \ln(m_x^2/(4\pi f)^2)$. A constant $\mathrm{tr}\,M$ therefore implies a constant $f_{\pi\mathrm{K}}$ up to logarithmic corrections. Note that due to Eq. (2.4) we also expect O(am) effects to violate the constancy of this combination.

With $f_{\pi\mathrm{K}}$ as a scale, we can define a second set of dimensionless variables

$$y_\pi = \frac{m_\pi^2}{(4\pi f_{\pi\mathrm{K}})^2} \qquad \text{and} \qquad y_{\mathrm{K}} = \frac{m_{\mathrm{K}}^2}{(4\pi f_{\pi\mathrm{K}})^2} \tag{2.6}$$

for which the linear combination $y_{\pi\mathrm{K}} = y_\pi/2 + y_{\mathrm{K}}$ is again constant in ChPT along our chiral trajectory.

Using the experimental values of the meson masses corrected for isospin breaking effects [14] and the PDG values for the decay constants [15], we use as input parameters

$$
\begin{aligned}
m_\pi &= 134.8(3)\mathrm{MeV}\,; \quad m_{\mathrm{K}} = 494.2(3)\ \mathrm{MeV} \\
f_\pi &= 130.4(2)\ \mathrm{MeV}\,; \quad f_{\mathrm{K}} = 156.2(7)\ \mathrm{MeV}\,.
\end{aligned}
\tag{2.7}
$$

4

2.2 Finite volume effects

The finite spatial volume of the lattices can affect the quantities we are interested in. A detailed study of these effects is planned in the future, but a general requirement is that one has to ensure $f_\pi L \gg 1$ and $m_\pi L \gg 1$ for them to be small.

For the lattices apart from H200 listed in Table 1, we have $L \geq 2.4$ fm and $m_\pi L > 4$ throughout. The chiral perturbation theory prediction [16, 17] indicates that the systematic effects on f_π and m_π are below our statistical uncertainties on the ensembles which enter our analysis, however, in some cases they are not completely negligible. The largest finite volume effect is on the N200 ensemble, where it amounts to 70% of the statistical error. We therefore apply the one-loop finite volume corrections to all data. The remaining effect, not accounted for by this correction, should be significantly below the statistical uncertainty and can therefore be neglected.

The H200 ensemble is excluded from the analysis, because the finite volume effect in the decay constant is too large. It is at the same physical parameters as the N202 ensemble, but with $L/a = 32$ instead of 48 and is therefore the only lattice with $L \approx 2$ fm. The measured finite volume effect between the two volumes in the decay constant is $-2.5(1.0)\%$, where ChPT predicts a -0.9% correction. While the accuracy of the data is not high enough for a detailed comparison, the correction beyond the ChPT prediction is to be significantly smaller for the larger volumes on which we base our computation.

3 Open boundaries and hadronic observables

Three types of fermionic observables are required for the scale setting in this paper: the masses and decay constants of the pseudoscalar mesons, as well as the PCAC quark masses. The open boundary conditions of the gauge field configurations do not pose a fundamental problem in the analysis due to the fact that the transfer matrix is not changed [18, 19]. Still some parts of the analysis have to be adapted because of the broken translational invariance at the boundaries at $x_0 = 0$ and $x_0 = T$. By construction, the boundary states share the quantum numbers of the vacuum and, if source or sink of the two-point functions come close to the boundaries, the whole tower of these states contributes to correlation functions.

As usual, pseudoscalar masses and decay constants are extracted from correlation functions of the pseudoscalar density $P^{rs} = \bar{\psi}^r \gamma_5 \psi^s$ and the improved axial vector current $A_\mu = \bar{\psi}^r \gamma_\mu \gamma_5 \psi^s + a c_A \tilde{\partial}_\mu P^{rs}$ with non-perturbatively tuned coefficient c_A [20]. The two-point functions

$$f_P^{rs}(x_0, y_0) = -\frac{a^6}{L^3} \sum_{\vec{x}, \vec{y}} \langle P^{rs}(x_0, \vec{x}) P^{sr}(y_0, \vec{y}) \rangle \,,$$

$$f_A^{rs}(x_0, y_0) = -\frac{a^6}{L^3} \sum_{\vec{x}, \vec{y}} \langle A_0^{rs}(x_0, \vec{x}) P^{sr}(y_0, \vec{y}) \rangle \,,$$

$$(3.1)$$

where r and s are flavor indices, are estimated with stochastic sources located on time slice y_0, for which we choose either $y_0 = a$ or $y_0 = T - a$. This choice and the general procedure are suggested by the comparison of various strategies in Ref. [21].

3.1 Excited states and boundary effects

To obtain the vacuum expectation values, we have to define the plateaux regions in which excited state contributions can be neglected. As in Ref. [22], the general strategy to define plateaux is divided in two steps. First, we perform preliminary fits including the first excited state, where the fit interval is chosen such that this model describes the data well by using a χ^2 test.

In the second step, only the function describing the ground state contribution is used, with the fit range given by the region where the excited state contribution as determined by the first fit is negligible compared to the statistical errors of the data.

From our measurements of f_P and f_A we observe, at fixed lattice spacing, that boundary effects increase as the up-down quark masses are lowered. This turns out to be particularly relevant for the quantity $R_{PS}(x_0, y_0)$ defined below in Eq. (3.4) where, according to our criterion for the definition of a plateau, boundary effects can be neglected starting from $x_0 \approx 3$ fm for pion masses around 200 MeV, as shown in Figure 1. Nevertheless, despite the fraction of the lattice which is discarded, we have been able to extract meson decay constants with one percent accuracy (and higher) on all ensembles, as reported in Table 2. Here, and all other cases presented, we use the statistical analysis method of Ref. [23], taking into account the autocorrelation of the data including contributions from the slowest observed modes of the Markov Chain Monte Carlo as determined in Ref. [1].

For the PCAC masses deviations from a flat behavior constitute a pure discretization effect. We have observed the largest ones at $\beta = 3.4$, where a plateau can be identified at distances of around 1.7 fm from the boundaries, while at $\beta = 3.7$ this distance shrinks to 0.7 fm.

3.2 Meson masses

In the presence of open boundary conditions, the pseudoscalar correlator f_P has the asymptotic behavior

$$f_P(x_0, y_0) = A_1(y_0)e^{-m_{PS}x_0} + A_2(y_0)e^{-m'x_0} + B_1(y_0)e^{-(E_{2PS}-m_{PS})(T-x_0)} + \dots , \quad (3.2)$$

for $T \gg x_0 \gg y_0$, where we included the contribution from the first excited state. The third exponential term originates from the first boundary excited state, a finite volume two pion state. In large volume, $E_{2PS} \approx 2m_{PS}$, leading to the sinh-like functional form presented in Ref. [19].

Taking into account the leading corrections from excited states for this formula, which are exponentially suppressed with the distance of the sink from the source
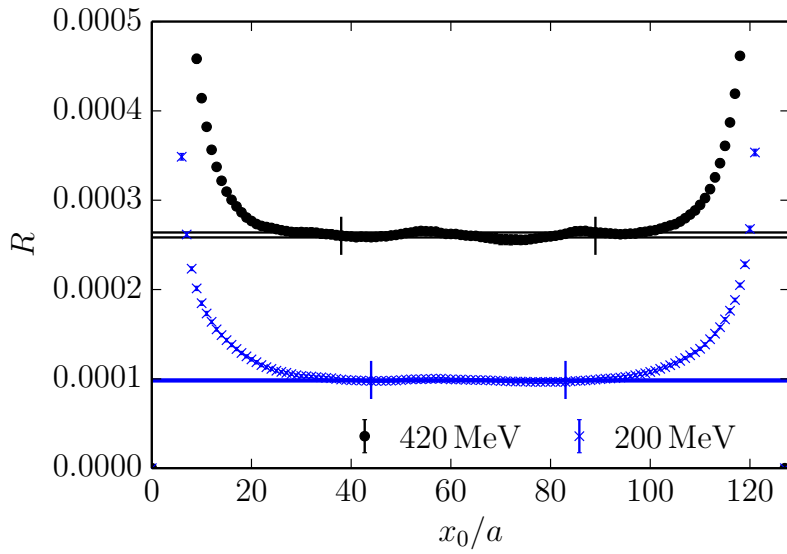
Figure 1: The effective quantity $R = R_{\mathrm{PS}}(x_0, a)$ defined in Eq. (3.4), from which the decay constants are extracted, for ensembles N202 and D200. Both of them share the same $\beta = 3.55$, but differ in the quark masses, the pion having a mass of $\approx 420\,\mathrm{MeV}$ for the former and $200\,\mathrm{MeV}$ for the latter. For the combined observable, the sources are at $y_0 = a$ and $y_0 = T - a$, with the sink varying over the temporal extent of the lattice. The horizontal lines indicate the plateau average and its uncertainty, the vertical lines the plateau ranges. Smaller pion mass leads to boundary effects reaching farther into the bulk.

and the boundaries, respectively, results in

$$am_{\text{eff}}(x_0) \equiv \log \frac{f_P(x_0)}{f_P(x_0 + a)} = am_{\text{PS}}(1 + c_1 e^{-E_1 x_0} + c_2 e^{-E_{2\text{PS}}(T - x_0)} + \dots), \quad (3.3)$$

with $E_1 = m' - m_{\text{PS}}$ and only c_1 and c_2 depending on the source position y_0. As discussed in the previous section, we determine the plateau range in x_0, where the exponential corrections can be safely neglected compared to the statistical uncertainties. The results of the plateau fits can be found in Table 2.

To check for possible systematics, also direct fits of Eq. (3.2) including terms of excited states have been tried, without going through the effective mass. The differences of the results are significantly below our statistical accuracy.

3.3 Decay constants and quark masses

The vacuum expectation values needed for the extraction of the decay constants are obtained from the plateaux in x_0 of the ratio (where we drop the flavor indices rs)

$$R_{\text{PS}}(x_0, y_0) = \left[\frac{f_A(x_0, y_0) \, f_A(x_0, T - y_0)}{f_P(T - y_0, y_0)} \right]^{1/2}. \quad (3.4)$$

This ratio is formed such that matrix elements of operators close to the boundary drop out. In this case, the plateaux are defined by fitting the ratios R_{PS} with

$$R_{\text{PS}}(x_0, y_0) = R(1 + c_1(y_0) \cosh[-E_1(T/2 - x_0)]), \quad (3.5)$$

since it is invariant under time reversal transformations. Once the relevant matrix element is known, the pseudoscalar decay constants are computed from

$$f_{\text{PS}} = Z_A(\tilde{g}_0) \left[1 + \bar{b}_A a \text{tr} \, M_q + \tilde{b}_A a m_{rs} \right] f_{\text{PS}}^{\text{bare}} \quad (3.6)$$

$$f_{\text{PS}}^{\text{bare}} = \sqrt{\frac{2}{m_{\text{PS}}}} R_{\text{PS}}^{\text{aver}}, \quad (3.7)$$

where $R_{\text{PS}}^{\text{aver}}$ is the plateau average of the ratio previously introduced.

The third observable we are interested in is the PCAC quark mass $m_{rs}(x_0, y_0) = \tilde{\partial}_{x_0} f_A^{rs}(x_0, y_0)/(2 f_P^{rs}(x_0, y_0))$ where $\tilde{\partial}_{x_0}$ is the symmetric derivative in time direction. With the same technique described for the effective mass in Sect. 3.2, plateaux in x_0 are also found for this quantity, which is then multiplicatively renormalized (up to $O(a^2)$ corrections) according to

$$m_{rs,\text{R}} = \frac{Z_A}{Z_P} \left[1 + (\bar{b}_A - \bar{b}_P) a \text{tr} \, M_q + (\tilde{b}_A - \tilde{b}_P) a m_{rs} \right] m_{rs}. \quad (3.8)$$

The present knowledge of the improvement coefficients[1] for the action that we used

---

[1] Note that in eq. (3.8) we have already replaced bare subtracted quark masses, which are multiplied by $b_A - b_P$, with their corresponding bare PCAC masses, thus leading to the $\tilde{b}_A$ and $\tilde{b}_P$ coefficients.

id	t_0	am_π	am_K	am_{12}	am_{13}	af_π	af_K
H101	2.8469(59)	0.18302(57)	0.18302(57)	0.009202(45)	0.009202(45)	0.06351(34)	0.06351(34)
	2.8619(56)	0.17979(17)	0.17979(17)	0.008893(36)	0.008893(36)	0.06296(37)	0.06296(37)
H102	2.8801(73)	0.15412(65)	0.19165(52)	0.006520(48)	0.010187(47)	0.06057(34)	0.06369(27)
	2.8861(54)	0.15306(23)	0.19068(16)	0.006428(35)	0.010091(39)	0.06053(31)	0.06358(26)
H105	2.8933(78)	0.12185(95)	0.20127(62)	0.003956(50)	0.011258(47)	0.05723(57)	0.06388(31)
	2.8920(74)	0.12151(34)	0.20166(23)	0.003952(46)	0.011304(36)	0.05752(59)	0.06432(28)
C101	2.9080(51)	0.09759(87)	0.20645(36)	0.002494(42)	0.011872(31)	0.05561(40)	0.06383(21)
	2.9044(39)	0.09901(36)	0.20708(11)	0.002566(29)	0.011935(25)	0.05573(38)	0.06390(21)
H400	3.635(13)	0.16345(66)	0.16345(66)	0.008228(36)	0.008228(36)	0.05690(37)	0.05690(37)
	3.662(12)	0.15896(28)	0.15896(28)	0.007786(63)	0.007786(62)	0.05631(52)	0.05631(52)
H402	3.558(16)	0.17727(62)	0.17727(62)	0.009779(44)	0.009779(44)	0.05887(41)	0.05887(41)
H200	5.150(25)	0.13717(76)	0.13717(76)	0.006856(30)	0.006856(30)	0.04704(43)	0.04704(43)
N202	5.164(16)	0.13407(43)	0.13407(43)	0.006855(16)	0.006855(16)	0.04829(20)	0.04829(20)
	5.166(15)	0.13382(20)	0.13382(20)	0.006832(39)	0.006832(36)	0.04829(21)	0.04829(21)
N203	5.1433(74)	0.11224(30)	0.14369(23)	0.004751(15)	0.007902(12)	0.04632(17)	0.04901(14)
	5.1427(80)	0.11233(16)	0.14377(11)	0.004761(26)	0.007912(26)	0.04639(18)	0.04906(14)
N200	5.1590(76)	0.09222(34)	0.15066(24)	0.003150(11)	0.008649(12)	0.04422(18)	0.04911(20)
	5.1600(76)	0.09197(20)	0.15053(11)	0.003137(22)	0.008636(19)	0.04432(19)	0.04915(20)
D200	5.1802(78)	0.06502(35)	0.15644(16)	0.001536(12)	0.009379(11)	0.04233(16)	0.04928(21)
	5.1761(82)	0.06611(30)	0.156912(86)	0.001591(16)	0.009436(17)	0.04253(18)	0.04943(20)
N300	8.576(30)	0.10630(34)	0.10630(34)	0.0055046(91)	0.0055046(91)	0.03790(20)	0.03790(20)
	8.596(27)	0.10376(16)	0.10376(16)	0.005237(47)	0.005237(37)	0.03770(23)	0.03770(23)
J303	8.613(20)	0.06514(35)	0.12015(19)	0.002053(17)	0.007204(33)	0.03424(24)	0.03854(37)
	8.637(24)	0.06259(28)	0.11879(11)	0.001884(44)	0.007027(67)	0.03399(36)	0.03845(50)

Table 2: Values of t_0, the pseudoscalar quark masses and decay constants as well as the PCAC masses. For each ensemble we give the measured values in the rows with the labels and in the row below the values after the shift to $\phi_4 = 1.11$.

is limited to one-loop[2] perturbation theory [25]

$$\tilde{b}_{\mathrm{A}} - \tilde{b}_{\mathrm{P}} = -0.0012 g_0^2 + O(g_0^4) \, ,$$
$$\tilde{b}_{\mathrm{A}} = 1 + 0.1174 g_0^2 + O(g_0^4) \, , \quad \bar{b}_{\mathrm{A}} = \bar{b}_{\mathrm{P}} = O(g_0^4) \, . \tag{3.9}$$

The finite renormalization factor Z_{A} has been computed using the Schrödinger Functional [26] and its chirally rotated variant [27]. We use the latter result due to its higher statistical accuracy, measured directly at the simulated values of g_0, thus neglecting terms of order $b_g g_0^4$. The non-perturbative running of the scale-dependent factor Z_{P} is not yet completed [28]. Hence, in the following we will consider only ratios of renormalized PCAC masses which do not depend on renormalization factors.

Starting from the leading matrix element of f_{P}, a second possibility to obtain the decay constants is based on the PCAC relation. The former can be obtained from a ratio similar to R_{PS} where the axial two point functions in the numerator are simply replaced by their corresponding f_{P}. For this quantity, however, we observed much stronger boundary contaminations and therefore we did not follow this strategy to compute the pseudoscalar decay constants.

4   Mass corrections

As we have seen above, it is necessary to control small corrections in the quark masses from the ones at which the simulations have been performed. This could be done by reweighting [29, 30], but here we only consider the leading corrections in a Taylor expansion. Since the required shifts are typically determined from the fit to the data, this has the advantage that we can include its effect easily in the full data analysis without need of interpolation between the measured points of a reweighting.

For a general function $f(\bar{A}_1(m), \ldots, \bar{A}_n(m))$ of expectation values of primary observables $\bar{A}_i = \langle A_i \rangle$, the derivative with respect to a parameter m of the theory reads

$$\frac{d}{dm} f = \sum_i \frac{\partial f}{\partial \bar{A}_i} \left[\langle \frac{\partial A_i}{\partial m} \rangle - \langle (A_i - \bar{A}_i)(\frac{\partial S}{\partial m} - \overline{\frac{\partial S}{\partial m}}) \rangle \right] \tag{4.1}$$

with S denoting the action of the theory. In the analysis we then use

$$f(m') \to f(m) + (m' - m) \frac{d}{dm} f(m) \tag{4.2}$$

neglecting higher order terms.

---

[2] Non-perturbatively determined values have become available while writing up the present analysis [24].
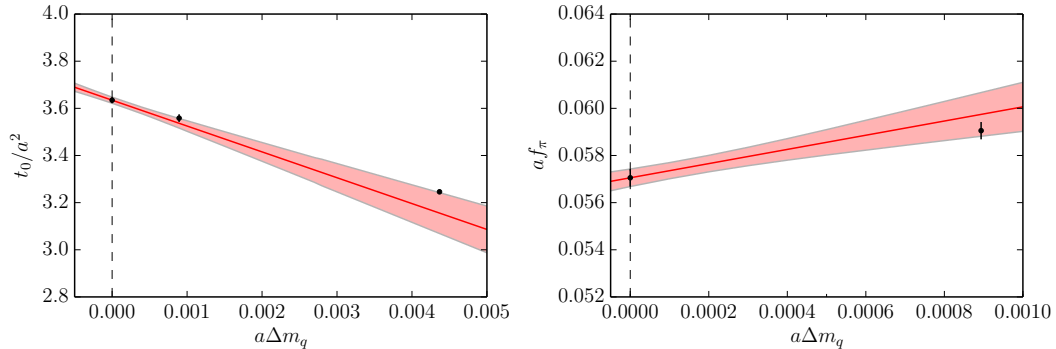
Figure 2: Examples of the mass shifts for the t_0 and f_π along the symmetric line $m_{\mathrm{ud}} = m_{\mathrm{s}}$ at $\beta = 3.46$. The data points correspond to the measurements on the ensembles H400, H401 and H402. The shaded bands give the linear approximation to the mass dependence starting from the leftmost point. Deviations from the linear approximation are smaller than the increase in the statistical uncertainties.

4.1 Measurements

For the measurement of the derivative we therefore need to compute the explicit derivative of the observable as well as the one of the action. If m is the bare quark mass, the derivative of hadronic correlation functions is easily evaluated as in

$$\partial_m \mathrm{tr} \Big[\frac{1}{D + m} \Gamma \frac{1}{D + m'} \Gamma' \Big] = -\mathrm{tr} \Big[\frac{1}{(D + m)^2} \Gamma \frac{1}{D + m'} \Gamma' \Big] . \qquad (4.3)$$

The numerical effort is limited: for each propagator a second inversion on the solution is necessary.

The second term in Eq. (4.1) contains the derivative of the action

$$- \partial_m \log \det(D + m) = -\mathrm{tr} \, (D + m)^{-1} , \qquad (4.4)$$

which can be evaluated using stochastic estimates of the trace. For our ensembles, we used 16 sources and found the noise introduced by them to be significantly inferior to the gauge noise of this observable.

4.2 Examples

To test the method we use ensembles at $\beta = 3.46$ which have been generated along the symmetric line H400, H401 and H402, where H402 has a sea quark mass which is roughly 19% larger than the one of H400 and H401 has roughly twice this mass. The results are displayed in Figure 2. We give the direct measurements on the three ensembles as well as the prediction indicated by the shaded band obtained from ensemble H400.

For t_0 we can shift roughly 9% in the quark mass before doubling the statistical uncertainty, for the decay constant this level is reached at a 5% shift. No deviations

from the linear approximation beyond the statistical error are visible in the displayed region. Since the shifts we apply in the following are smaller than those, we assume that the systematic error from dropping higher orders in the Taylor expansion can be neglected compared to the increase in statistical uncertainty.

5 Chiral and continuum extrapolation

There is no unique choice of chiral trajectory in the m_{ud}–m_{s} plane along which one moves as the pion mass is changed, as there is no unique choice of matching condition between different lattice spacings. These choices, however, have an impact on the ease with which the extrapolation to physical quark masses and to the continuum can be performed.

5.1 Chiral trajectory

As already mentioned above, the chiral trajectories defined by $\text{tr}M_{\text{q}} = \text{const}$ lead to discretization effects of $\text{O}(am)$ given in Eq. (2.4). To avoid them, an improved proxy for the quark mass is needed. There are basically two options: the PCAC quark masses and the meson masses. The former has the advantage that a trajectory defined through a constant sum of these quark masses automatically leads to a constant coefficient of b_{g} in Eq. (2.2). The disadvantage is that the improvement coefficients $b_{\text{A}} - b_{\text{P}}$ and $\tilde{b}_{\text{A}} - \tilde{b}_{\text{P}}$ are known only perturbatively. However, our masses are small and so are the one-loop values of these combinations.

We opt for using the sum of the mass squares of pseudoscalar mesons $m_{\text{K}}^2 + \frac{1}{2}m_{\pi}^2$, which in leading order of Chiral Perturbation Theory is proportional to the sum of the three light quark masses. While these do not introduce any discretization effects at $\text{O}(a)$, it might introduce a small variation of the improved coupling, since the sum of quark masses varies due to higher order effects in ChPT. As we will see below, on a chiral trajectory defined through a constant $\phi_4 = 8t_0(m_{\text{K}}^2 + \frac{1}{2}m_{\pi}^2)$ also the sum of the renormalized quark masses is constant on the per-cent level. We can therefore safely assume that the effect of a variation in the term coming with b_{g} can be neglected.

5.2 Strategy 1

The obvious extension of the strategy used in the planning of the simulation is to continue with t_0 as a scale parameter, i.e. finding the physical value of ϕ_4 along which we move towards the chiral limit. Since the physical value of t_0 is not known beforehand, we determine it implicitly from another dimensionful observable.

The analysis therefore starts by assuming a certain physical value of $t_0 = \tilde{t}_0$. Together with Eq. (2.7), this defines the target point $(\tilde{\phi}_2, \tilde{\phi}_4)$ at which we can read off physical results of the calculations. Starting from the simulated ensembles, shifts along the line $\Delta m_{\text{u}} = \Delta m_{\text{d}} = \Delta m_{\text{s}}$ are now performed to reach $\tilde{\phi}_4$. This is the

direction in which $\mathrm{tr}M_\mathrm{q}$ changes fastest and therefore the effects due to the truncation of the Taylor expansion are expected to be smallest at the target $\tilde{\phi}_4$. As an intermediate result we get values of $\sqrt{t_0}/a$, $af_{\pi\mathrm{K}}(\phi_2)$ and their product at constant $\phi_4 = \tilde{\phi}_4$, which now have to be extrapolated to $\tilde{\phi}_2$.

For this extrapolation we use two different functional forms, one given by NLO ChPT, the other a Taylor expansion around the symmetric point. As noted in Ref. [31], along the line adopted in our simulations, the linear term in the quark mass does not contribute to the Taylor expansion and we can therefore use $F_\mathrm{T}^\mathrm{cont}(\phi_2) = c_0 + c_1(\phi_2 - \phi_2^\mathrm{sym})^2$.

The ChPT formula $F_\chi(\phi_2)$ can easily be derived from Eq. (2.5). Note that in NLO ChPT t_0 is constant along our trajectory at this order [32] and we have a straightforward relation between ϕ_2, ϕ_4 and the meson masses. At NLO, the ratios are therefore unambiguously given by the logarithms predicted by ChPT

$$\frac{\sqrt{t_0}f_{\pi\mathrm{K}}}{(\sqrt{t_0}f_{\pi\mathrm{K}})^\mathrm{sym}} = \frac{f_{\pi\mathrm{K}}}{(f_{\pi\mathrm{K}})^\mathrm{sym}} = 1 - \frac{7}{6}(L_\pi - L_\pi^\mathrm{sym}) - \frac{4}{3}(L_\mathrm{K} - L_\mathrm{K}^\mathrm{sym}) - \frac{1}{2}(L_\eta - L_\eta^\mathrm{sym}). \quad (5.1)$$

These continuum relations are augmented by a term to account for the leading discretization effects. In general, we adopt

$$\sqrt{t_0}f_{\pi\mathrm{K}} = F_{\mathrm{T}/\chi}^\mathrm{cont}(\phi_2) + c_{T/\chi}\frac{a^2}{t_0^\mathrm{sym}} \quad (5.2)$$

and will see below that our data is well compatible with this ansatz.

One result is a value of $\sqrt{t_0}f_{\pi\mathrm{K}}$ at $\tilde{\phi}_2$ and $\tilde{\phi}_4$ as defined by $\tilde{t}_0$. Using the physical value of $f_{\pi\mathrm{K}}$, this gives a value of t_0 in physical units. The final goal is to find the fixed point, at which this value agrees with the input $\tilde{t}_0$. This then defines the physical value of t_0 and in turn the physical value of ϕ_4.

As we see from Figure 3, both the ChPT formula as well as the Taylor expansion, fitted to our data, hardly differ in the range of our points. Also at physical quark masses, the difference amounts to roughly half the statistical uncertainty. Taking into account the full propagation of the errors through this fixed point condition, we therefore arrive at physical values of

$$\phi_4^\mathrm{phys} = 1.11(2) \qquad \text{and} \qquad \sqrt{8t_0^\mathrm{phys}} = 0.413(4)\,\mathrm{fm} \quad (5.3)$$

for the ChPT ansatz, while for the quadratic extrapolation formula one gets

$$\phi_4^\mathrm{phys} = 1.12(2) \qquad \text{and} \qquad \sqrt{8t_0^\mathrm{phys}} = 0.415(3)\,\mathrm{fm}. \quad (5.4)$$

The difference between the two results is $-0.0017(8)$, i.e. below the statistical accuracy. For convenience, we give the values of our observables shifted to $\phi_4 = 1.11(2)$ in Table 2. Including the systematic uncertainty of the chiral extrapolation, we therefore get

$$\sqrt{8t_0^\mathrm{phys}} = 0.414(4)(1)\,\mathrm{fm} \quad (5.5)$$
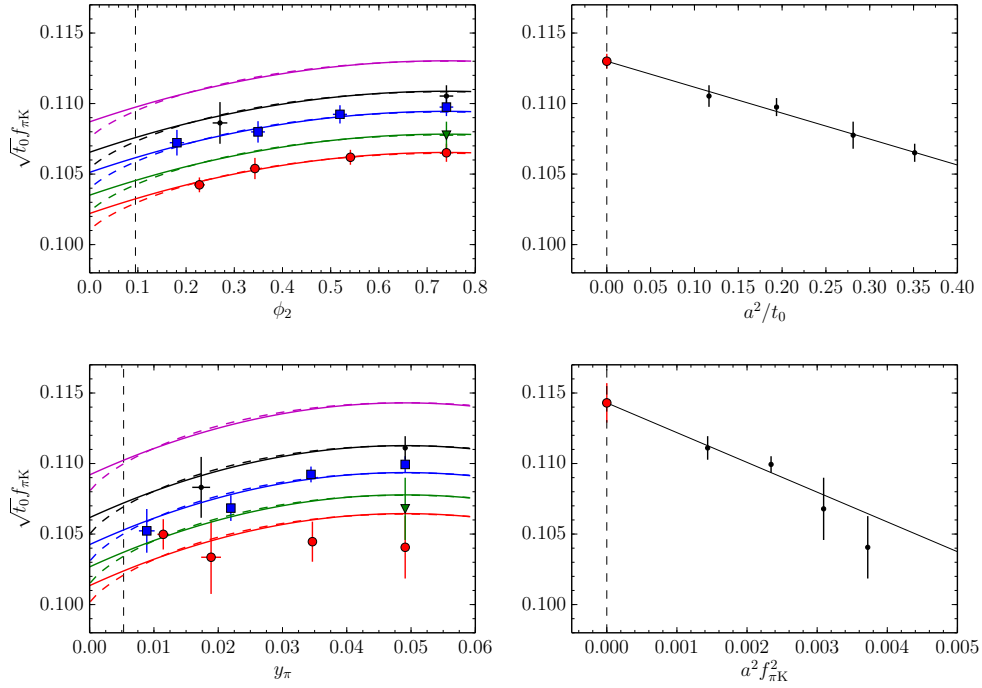
13

Figure 3: The dimensionless quantity $\sqrt{t_0}f_{\pi K}$ along the line $\phi_4 = 1.110$ in the top row, along the line of $y_{\pi K} = 0.074$ in the bottom row. In the left panels, we present all measurements as a function of ϕ_2 together with the fit result of the quadratic function (solid) and the ChPT Eq. (5.1). In the right panel the continuum extrapolation of the data at the symmetric point is shown. We observe discretization effects up to 7% for the coarsest lattice spacing.

β	$t_0^\star/a^2$	$a[\mathrm{fm}]$
3.4	2.860(10)(02)	0.08654(91)(21)
3.46	3.659(15)(02)	0.07650(80)(18)
3.55	5.164(17)(02)	0.06440(65)(15)
3.7	8.595(29)(02)	0.04992(48)(11)

Table 3: Lattice spacings from strategy 1 set by t_0 at the symmetric point and physical value of ϕ_4 as given in Eq. (5.5). Note the numbers in the second column are weakly correlated, whereas the values of the lattice spacings have strong correlations due to Eq. (5.6).

as final result of this strategy. The lattice spacing can now be set with $t_0^\star/a^2 \equiv t_0^{\mathrm{sym}}/a^2$ with $\phi_4 = \phi_4^{\mathrm{phys}}$. The corresponding values are given in Table 3.

In Eq. (5.5) we report the result for t_0 at physical quark masses. For scale setting, an alternative strategy is to use its value at the symmetric point given by $\phi_4 = \phi_4^{\mathrm{phys}}$. For this we fit Eq. (5.2) to $\sqrt{t_0^{\mathrm{sym}}} f_{\pi K}(\phi_2)$ with the same condition on ϕ_4. This analysis renders

$$\sqrt{8t_0^{\mathrm{sym}}} = 0.413(5)(1)\,\mathrm{fm}\,, \tag{5.6}$$

which is compatible with the above results. This reflects the small deviation from unity in the ratio t_0/t_0^{sym}.

5.3 Strategy 2

In the second strategy, we use $f_{\pi K}$ to set the scale, shifting each simulated lattice such that $y_{\pi K}$ equals its physical value $y_{\pi K}^{\mathrm{phys}} = 0.07363$. This strategy is simpler since its physical value is known, see Eq. (2.7). To set the lattice spacing one would compute $af_{\pi K}$ along the line of constant $y_{\pi K}$.

The disadvantage of this approach is that the parameters of our ensembles are farther away from this chiral trajectory and therefore require larger shifts. This increases the statistical uncertainties and also potential higher order effects in the Taylor expansion, which we neglect. To show which accuracy can be reached with the current data, $\sqrt{t_0} f_{\pi K}$ is plotted after the shift to physical $y_{\pi K}$ in the bottom plots of Figure 3. As we can see, the statistical uncertainties are significantly larger than the ones encountered in Strategy 1, such that the applicability of the linear correction terms alone is no longer clear. We therefore do not consider this strategy to be competitive on the current data.

Employing the same analysis strategy as in the previous section, using a polynomial function and the one given by ChPT, we arrive at $\sqrt{8t_0^{\mathrm{phys}}} = 0.417(9)\,\mathrm{fm}$ for the former and $\sqrt{8t_0^{\mathrm{phys}}} = 0.416(10)\,\mathrm{fm}$ for the latter.

The advantage of the strategy for the scale setting is a direct value of the lattice spacing from $f_{\pi K} = 147.6(5)\,\mathrm{MeV}$ at the physical point. This leads to $a =$

$0.0790(11)\,\mathrm{fm}$, $0.071(2)\,\mathrm{fm}$, $0.0613(9)\,\mathrm{fm}$ and $0.0481(8)\,\mathrm{fm}$ for $\beta = 3.4$, 3.46, 3.55 and 3.7, respectively. The difference to the results in the previous section is a discretization effect, which is already visible in the plots on the right hand side of Figure 3.

5.4   Discretization effects

Because of the large statistical error encountered in strategy 2, we will now restrict ourselves to the data obtained with the first strategy. One assumption entering the analysis presented above is that the data presented here can be described by the leading discretization effects of order a^2 at the level of statistical accuracy. To get a handle on this, in Figure 3 the dimensionless product $\sqrt{t_0}f_{\pi K}$ is displayed as a function of a^2/t_0 at the symmetric point given by $\phi_4 = \phi_4^{\mathrm{phys}}$. As we can see, the data exhibits no deviation from a linear behavior, supporting further the assumption made in the ansatz 5.2.

5.5   Chiral extrapolation

The effect of the chiral extrapolation is best studied by forming ratios between the value of the observable at the symmetric point and the one at parameters closer to the chiral limit but at the same lattice spacing. In these ratios, some of the lattice systematics cancels such that for the chiral effects a high sensitivity can be reached.

The original ensembles are along trajectories of constant sum of bare quark masses, matched at the 1% level using ϕ_4 at the symmetric point. The results for the ratios can be found in the left column of Figure 4. As we can see from the lower plot, the sum of renormalized quark masses is not constant. These masses have been improved with a non-perturbatively determined c_{A}, effects of the b-terms have been neglected. The fact that the renormalized sum is not constant is a discretization effect. At $\beta = 3.4$ their size is so large that they cannot be attributed to contributions linear in the quark masses alone; higher order contributions are noticeable at this coarse lattice spacing.

In the right column of this plot we see the effect of the shift to a constant $\phi_4 = 1.11$, which is close to the physical value. The renormalized quark mass is now constant on the per-cent level even for the coarsest lattice spacing, with the remaining effects compatible with reasonable values of the b-terms. This also justifies our choice of aiming for a constant ϕ_4 versus a constant $\mathrm{tr}M^{\mathrm{R}}$: the difference between these two options cannot be resolved by the statistical accuracy of the data and in any case is limited to the per-cent level.

The effect on the ratios of t_0 and $f_{\pi K}$ is less dramatic. In agreement with the expectation both based on the Taylor expansion of a flavor symmetric quantity around the symmetric point [6,31] and ChPT [32], the chiral corrections are tiny, in particular for the finer lattices. At the coarsest lattice spacing, some deviation from the constant behavior is still observed, which is reduced by the shift to $\phi_4 =$ const.

The chiral effect in $f_{\pi K}$ is more noticeable, with a correction on the level of $3-4\%$ to the physical light quark mass point. Notice, that our data agrees well with the logarithms predicted by ChPT in Eq. (2.5).

6 Conclusions

Many observables can be used as a lattice scale, all agree up to effects which come from an incomplete description of Nature. Here we neglect for instance quarks heavier than the strange, electromagnetism and isospin breaking. The main strategy pursued in the present study is to use t_0 as an intermediate scale, with the approach to the chiral limit along lines of constant $\phi_4 = 8t_0(m_K^2 + m_\pi^2/2)$. Using $f_{\pi K}$ as physical input, this allows the determination of the physical value of t_0. This strategy is preferred due to the currently available ensembles in the CLS effort, because the ensembles have been tuned with t_0 as a scale.

Starting with statistical accuracies for the decay constants on the level of 0.5%, we are able to determine t_0 at the per-cent level

$$\sqrt{8t_0} = 0.414(4)(1)\,\text{fm}\,. \tag{6.1}$$

This compares well to previous determinations using 2+1 flavors by the BMW collaboration [33] that quotes $\sqrt{8t_0} = 0.414(7)\,\text{fm}$ and is also within 2σ of the QCDSF result [6] $0.427(7)\,\text{fm}$ as well as RBC-UKQCD's value [34] of $0.407(2)\,\text{fm}$. Using 2+1+1 dynamical flavors the MILC [35] and HPQCD [36] collaborations find $\sqrt{8t_0} = 0.4005\binom{22}{11}\,\text{fm}$ and $0.4016(22)\,\text{fm}$, respectively, which might be an effect of the number of flavors in the sea as is the two-flavor result $\sqrt{8t_0} = 0.434(3)\,\text{fm}$ [37].

With additional ensembles becoming available, the analysis presented here will improve. However, even the accuracies of the current study will already allow to reach a good precision in many physics projects.
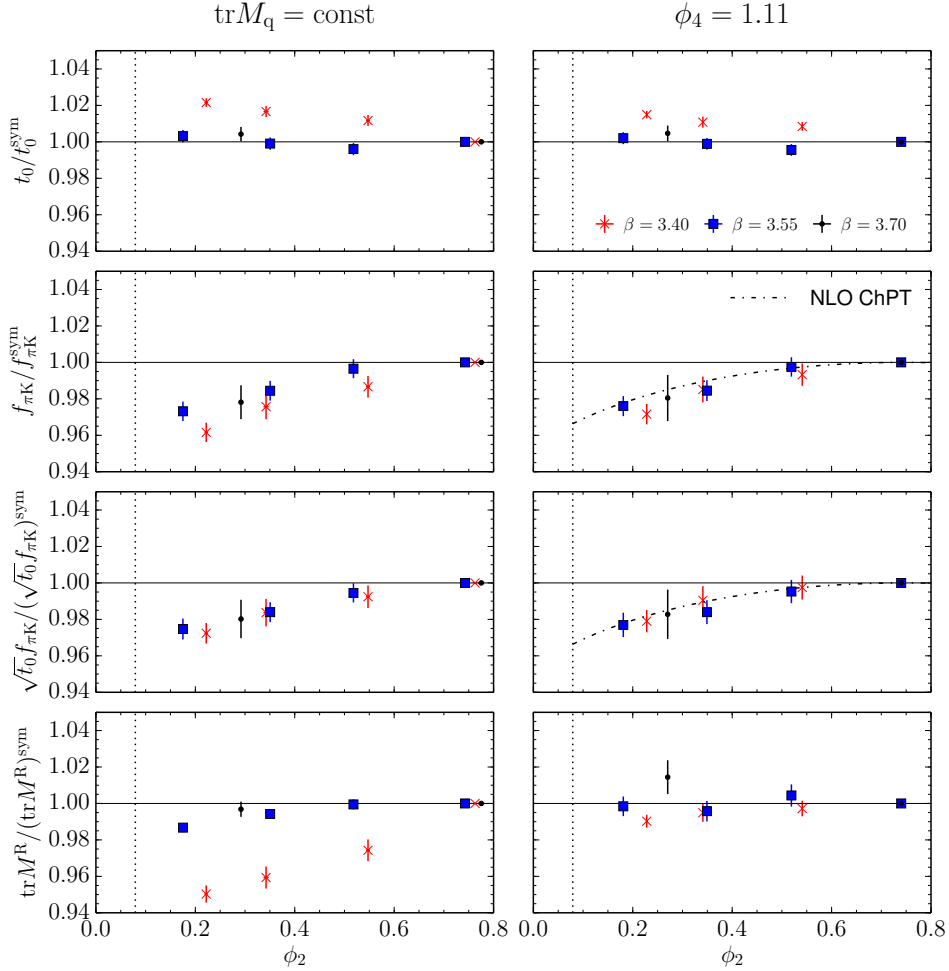
Figure 4: Effect of the chiral extrapolation on t_0, $f_{\pi K}$ and the sum of perturbatively improved PCAC masses. The data is always normalized by the symmetric point. In the left column, the data as measured on the simulated ensembles, where $\mathrm{tr}\,(M_{\mathrm{q}})$ is kept fixed. On the right after the shifts to a constant $\phi_4 = 1.11$ has been applied. In particular for the quark mass sum we observe a significant effect. While the violation of $\mathrm{tr}\,(M_{\mathrm{q}}^{\mathrm{R}})$=const before the shift cannot be explained by effects linear in the lattice spacing, we observe that constant ϕ_4 implies constant renormalized quark mass to high accuracy.

References

[1] M. Bruno et al., *Simulation of QCD with $N_f = 2 + 1$ flavors of non-perturbatively improved Wilson fermions*, *JHEP* **02** (2015) 043, [1411.3982].

[2] M. Lüscher, *Properties and uses of the Wilson flow in lattice QCD*, *JHEP* **1008** (2010) 071, [1006.4518].

[3] D. Toussaint and C. T. H. Davies, *The Omega- and the strange quark mass*, *Nucl. Phys. Proc. Suppl.* **140** (2005) 234–236, [hep-lat/0409129].

[4] FERMILAB LATTICE, HPQCD, UKQCD, MILC collaboration, C. T. H. Davies et al., *High precision lattice QCD confronts experiment*, *Phys. Rev. Lett.* **92** (2004) 022001, [hep-lat/0304004].

[5] R. Sommer, *A New way to set the energy scale in lattice gauge theories and its applications to the static force and alpha-s in SU(2) Yang-Mills theory*, *Nucl.Phys.* **B411** (1994) 839–854, [hep-lat/9310022].

[6] V. G. Bornyakov et al., *Wilson flow and scale setting from lattice QCD*, 1508.05916.

[7] ALPHA collaboration, M. Bruno, J. Finkenrath, F. Knechtli, B. Leder and R. Sommer, *Effects of Heavy Sea Quarks at Low Energies*, *Phys. Rev. Lett.* **114** (2015) 102001, [1410.8374].

[8] J. Bulava and S. Schaefer, *Improvement of $N_f = 3$ lattice QCD with Wilson fermions and tree-level improved gauge action*, *Nucl.Phys.* **B874** (2013) 188–197, [1304.7093].

[9] G. S. Bali, E. E. Scholz, J. Simeth and W. Söldner, *Lattice simulations with $N_f = 2 + 1$ improved Wilson fermions at a fixed strange quark mass*, 1606.09039.

[10] K. G. Wilson, *Confinement of Quarks*, *Phys.Rev.* **D10** (1974) 2445–2459.

[11] W. Bietenholz et al., *Tuning the strange quark mass in lattice simulations*, *Phys.Lett.* **B690** (2010) 436–441, [1003.1114].

[12] T. Bhattacharya, R. Gupta, W. Lee, S. R. Sharpe and J. M. Wu, *Improved bilinears in lattice QCD with non-degenerate quarks*, *Phys.Rev.* **D73** (2006) 034504, [hep-lat/0511014].

[13] J. Gasser and H. Leutwyler, *Chiral Perturbation Theory: Expansions in the Mass of the Strange Quark*, *Nucl. Phys.* **B250** (1985) 465–516.

[14] S. Aoki et al., *Review of lattice results concerning low-energy particle physics*, 1607.00299.

[15] PARTICLE DATA GROUP collaboration, K. A. Olive et al., *Review of Particle Physics*, *Chin. Phys.* **C38** (2014) 090001.

[16] J. Gasser and H. Leutwyler, *Light Quarks at Low Temperatures*, *Phys. Lett.* **B184** (1987) 83.

[17] G. Colangelo, S. Durr and C. Haefeli, *Finite volume effects for meson masses and decay constants*, *Nucl. Phys.* **B721** (2005) 136–174, [`hep-lat/0503014`].

[18] M. Lüscher and S. Schaefer, *Lattice QCD without topology barriers*, *JHEP* **1107** (2011) 036, [`1105.4749`].

[19] M. Lüscher and S. Schaefer, *Lattice QCD with open boundary conditions and twisted-mass reweighting*, *Comput.Phys.Commun.* **184** (2013) 519–528, [`1206.2809`].

[20] ALPHA collaboration, J. Bulava, M. Della Morte, J. Heitger and C. Wittemeier, *Non-perturbative improvement of the axial current in $N_f=3$ lattice QCD with Wilson fermions and tree-level improved gauge action*, *Nucl. Phys.* **B896** (2015) 555–568, [`1502.04999`].

[21] M. Bruno, P. Korcyl, T. Korzec, S. Lottini and S. Schaefer, *On the extraction of spectral quantities with open boundary conditions*, *PoS* **LATTICE2014** (2014) 089, [`1411.5207`].

[22] ALPHA collaboration, P. Fritzsch, F. Knechtli, B. Leder, M. Marinkovic, S. Schaefer et al., *The strange quark mass and Lambda parameter of two flavor QCD*, *Nucl.Phys.* **B865** (2012) 397–429, [`1205.5380`].

[23] ALPHA collaboration, S. Schaefer, R. Sommer and F. Virotta, *Critical slowing down and error analysis in lattice QCD simulations*, *Nucl.Phys.* **B845** (2011) 93–119, [`1009.5228`].

[24] P. Korcyl and G. S. Bali, *Non-perturbative determination of improvement coefficients using coordinate space correlators in $N_f = 2 + 1$ lattice QCD*, `1607.07090`.

[25] Y. Taniguchi and A. Ukawa, *Perturbative calculation of improvement coefficients to $O(g**2a)$ for bilinear quark operators in lattice QCD*, *Phys.Rev.* **D58** (1998) 114503, [`hep-lat/9806015`].

[26] J. Bulava, M. Della Morte, J. Heitger and C. Wittemeier, *Nonperturbative renormalization of the axial current in $N_f = 3$ lattice QCD with Wilson fermions and a tree-level improved gauge action*, *Phys. Rev.* **D93** (2016) 114513, [`1604.05827`].

[27] M. Dalla Brida, K. Korzec, S. Sint and P. Vilaseca, *A precise determination of the non-singlet axial and vector currents renormalization constants for $O(a)$ improved Wilson-fermions, in preparation* .

[28] I. Campos, P. Fritzsch, C. Pena, D. Preti, A. Ramos and A. Vladikas, *Prospects and status of quark mass renormalization in three-flavour QCD*, *PoS* **LATTICE2015** (2016) 249, [`1508.06939`].

[29] A. Hasenfratz, R. Hoffmann and S. Schaefer, *Reweighting towards the chiral limit*, *Phys.Rev.* **D78** (2008) 014515, [0805.2369].

[30] J. Finkenrath, F. Knechtli and B. Leder, *One flavor mass reweighting in lattice QCD*, *Nucl.Phys.* **B877** (2013) 441–456, [1306.3962].

[31] W. Bietenholz et al., *Flavour blindness and patterns of flavour symmetry breaking in lattice simulations of up, down and strange quarks*, *Phys. Rev.* **D84** (2011) 054509, [1102.5300].

[32] O. Bär and M. Golterman, *Chiral perturbation theory for gradient flow observables*, *Phys.Rev.* **D89** (2014) 034505, [1312.4999].

[33] S. Borsanyi et al., *High-precision scale setting in lattice QCD*, *JHEP* **1209** (2012) 010, [1203.4469].

[34] RBC, UKQCD collaboration, T. Blum et al., *Domain wall QCD with physical quark masses*, *Phys. Rev.* **D93** (2016) 074505, [1411.7017].

[35] MILC collaboration, A. Bazavov et al., *Gradient flow and scale setting on MILC HISQ ensembles*, *Phys. Rev.* **D93** (2016) 094510, [1503.02769].

[36] R. Dowdall, C. Davies, G. Lepage and C. McNeile, V_{us} *from* π *and* K *decay constants in full lattice QCD with physical u, d, s and c quarks*, *Phys.Rev.* **D88** (2013) 074504, [1303.1670].

[37] M. Bruno and R. Sommer, *On the* N_f*-dependence of gluonic observables*, *PoS* **LATTICE2013** (2013) 321, [1311.5585].